

# In-Situ Formation of Co Particles Encapsulated by Graphene Layers

**Minjeong Lee**

Gyeongsang National University

**Gyutae Kim**

Gyeongsang National University

**Gyu Hyun Jeong**

Gyeongsang National University

**Aram Yoon**

Ulsan National Institute of Science and Technology

**Zonghoon Lee**

Ulsan National Institute of Science and Technology

**Gyeong Hee Ryu** (✉ [gh.ryu@gnu.ac.kr](mailto:gh.ryu@gnu.ac.kr))

Gyeongsang National University <https://orcid.org/0000-0002-8992-8694>

---

## Research Article

**Keywords:** Co particle, encapsulation, graphene, Co(OH)<sub>2</sub>, STEM

**Posted Date:** May 31st, 2022

**DOI:** <https://doi.org/10.21203/rs.3.rs-1669649/v1>

**License:** © ⓘ This work is licensed under a Creative Commons Attribution 4.0 International License.

[Read Full License](#)

---

# In-Situ Formation of Co Particles Encapsulated by Graphene Layers

Minjeong Lee,<sup>1</sup> Gyutae Kim,<sup>1</sup> Gyu Hyun Jeong,<sup>1</sup> Aram Yoon,<sup>2,3</sup> Zonghoon Lee<sup>2,3</sup> and Gyeong Hee Ryu<sup>1\*</sup>

- 1 School of Materials Science and Engineering, Gyeongsang National University, Jinju, 52828 Republic of Korea
- 2 Department of Materials Science and Engineering, Ulsan National Institute of Science and Technology (UNIST), Ulsan 44919, Republic of Korea
- 3 Center for Multidimensional Carbon Materials, Institute for Basic Science (IBS), Ulsan 44919, Republic of Korea

\* Correspondence: [gh.ryu@gnu.ac.kr](mailto:gh.ryu@gnu.ac.kr)

## Abstract

The process of encapsulating cobalt nanoparticles using graphene layers is mainly direct pyrolysis. The encapsulation structure of hybrids prepared in this way improves the catalyst stability, which greatly reduces the leaching of non-metals and prevents metal nanoparticles from growing beyond a certain size. In this study, cobalt particles surrounded by graphene layers were formed by increasing the temperature in a transmission electron microscope, and they were analyzed using scanning transmission electron microscopy (STEM). Synthesized cobalt hydroxide nanosheets were used to obtain cobalt particles using an in-situ heating holder inside a TEM column. The cobalt nanoparticles are surrounded by layers of graphene, and the number of layers increases as the temperature increases. The interlayer spacing of the graphene layers was also investigated using atomic imaging. The success achieved in the encapsulation of metallic nanoparticles in graphene layers paves the way for the design of highly active and reusable heterogeneous catalysts for more challenging molecules.

## Keywords

Co particle, encapsulation, graphene, Co(OH)<sub>2</sub>, STEM

## Introduction

Metallic catalysts play a dominant role in industrial applications and the development of catalysts using base metals [Jagedeesh et al.; Meffere et al.; Jagadeesh et al.; Czaplik et al.; Zhang et al.] is prevalent because of their distinct electronic structures [Friedfeld et al.] and magnetic properties. In addition, a series of novel heterogeneous catalyst systems using noble metal catalysts [Rahi et al.; Le et al.; Ren et al.; Yan et al.; Ge et al.] have been developed, but noble metals have major drawbacks such as lack of selectivity and low resistance to functional groups. [Corma et al.]

In recent years, multi-metal catalysts made by bonding different transition metals have come into prominence. [Sammis et al.; Toyofuku et al.; Hashmi et al.; Chinchilla et al.] The driving force behind these efforts is the discovery of more efficient approaches for the synthesis of complex molecules with superior chemical and stereoselectivity that are not accessible through the use of monospecific catalyst systems. The development of these catalysts maximized compatibility while exploiting the benefits of catalysis. Furthermore, transition metals are predominantly applied to find more valuable chemical transformations. This growing interest has led to advances in the field focusing on how the reactivity of transition metal catalysts can be tuned. In addition to this, a strategy has been derived to create metal nanoparticles encapsulated in polymorphic carbon shells. [Yao et al.; Galakhov et al.; Liu et al.] The main advantage of encapsulated structures is the ability to tune the electronic structure of metal nanoparticles and tightly control the aggregation of nanoparticles. [Chen et al.; Tian et al.] In addition, encapsulation of metal nanoparticles within a porous carbon shell allows for easy access to the catalytically active sites and greatly inhibits mass transfer restrictions. [Wu et al.]

Recently, Co encapsulated in a carbon matrix has been developed for various reactions such as catalytic hydrogenation and oxygen reduction reaction. [Wei et al.; Liu et al.; Peng et al.; Wei et al.] Hybrid Co particles specifically designed to be encapsulated in a carbon material serve as an efficient, selective, and potent catalyst. The interface between the encapsulated Co particles and the graphene layer determines the structural and chemical properties. For metal/graphene systems, interfaces have also been focused on applying graphene to electronic devices where graphene is in contact with metal electrodes and wires. [Rosei et al.; Nagashima et al.; Gamo et al.; Abild-Pedersen et al.; Wang et al.; Gruneis et al.] Because these Co/graphene interfaces are two-dimensional internal structures, transmission electron microscopy (TEM) is the most useful method to investigate them. Herein, we report the formation of Co particles

encapsulated by graphene layers, which were induced using an in-situ TEM heating holder in a TEM column. We used synthesized  $\text{Co}(\text{OH})_2$  nanosheets and converted them into Co particles. The carbon matrix, which remained amorphous, was transformed into graphene layers surrounding the Co particles at high temperatures (over 800 °C). Interestingly, the number of graphene layers increases when heated to above 1000 °C. The whole process was analyzed using high-resolution STEM.

## Results and Discussion

cobalt hydroxide can be synthesized as nanosheets as shown in Figure 1a. Their chemical bonding states were confirmed using x-ray photoelectron spectroscopy (XPS) to consist of mainly cobalt hydroxide with some cobalt oxides (Figure 1b). We transferred the specimen onto a heating chip to induce a heating pulse into the specimen. The morphology and structure of the nanosheets were investigated using high-resolution scanning transmission electron microscopy (HR-STEM). Figure 1c shows a high-resolution image of the synthesized nanosheet, which is visualized as an amorphous phase (Figure 1c). When the heating pulse is applied to them, the amorphous nanosheets transform into crystalline cobalt particles above 500 °C (Figure 1d).

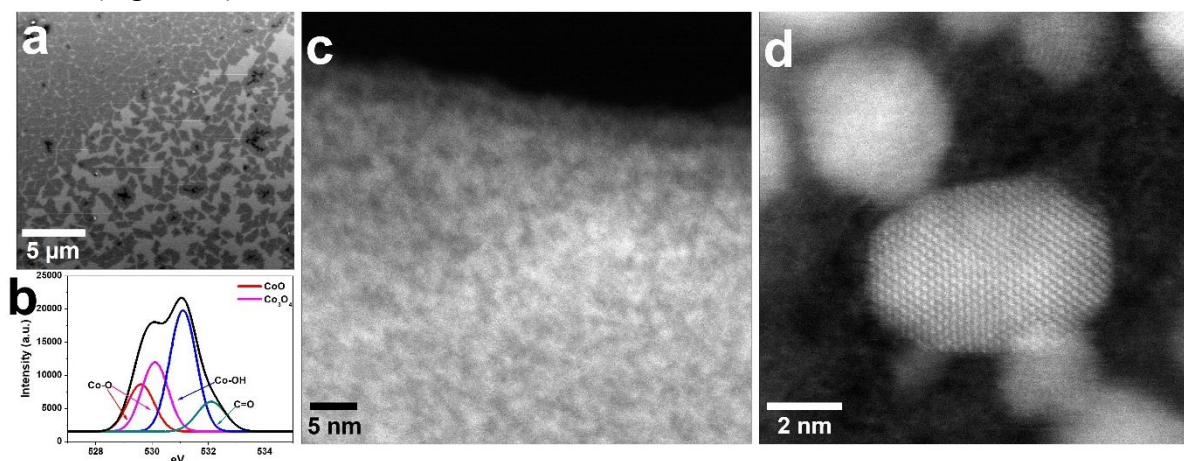


**Figure 1.** (a) and (b) SEM image and XPS spectra of the synthesized  $\text{Co}(\text{OH})_2$  nanosheets. (c) and (d) ADF-STEM images showing the nanosheet and Co particles formed using a heating holder.

When the temperature increases to 1100 °C, the nanosheets progressively transform as shown in Figures 2a to c, which are successive high angle annular dark field (HAADF)-STEM images showing the overall transformation behavior of the sheet in the same region. The transformation initiation is not implemented in only a specific area, but occurs in the entire sheet area to which temperature is applied, and Co atoms constituting  $\text{Co}(\text{OH})_2$  are aggregated to form a large amount of Co particles. When heated to 500 °C, Co particles are formed as shown in Figure 1, and the hydrocarbons remaining on the surface of the  $\text{Co}(\text{OH})_2$  nanosheet form a thin film as shown in Figure 2c. Figure 2d shows the HAADF-STEM image of the Co particles with a thin carbon film at 500 °C. Above 800 °C, the carbon film begins to crystallize gradually, and carbon layers (graphene layers) are formed at the edge of the Co particle (Figure 2e). The Co particles encapsulated by graphene layers are visualized in Figure 2f.

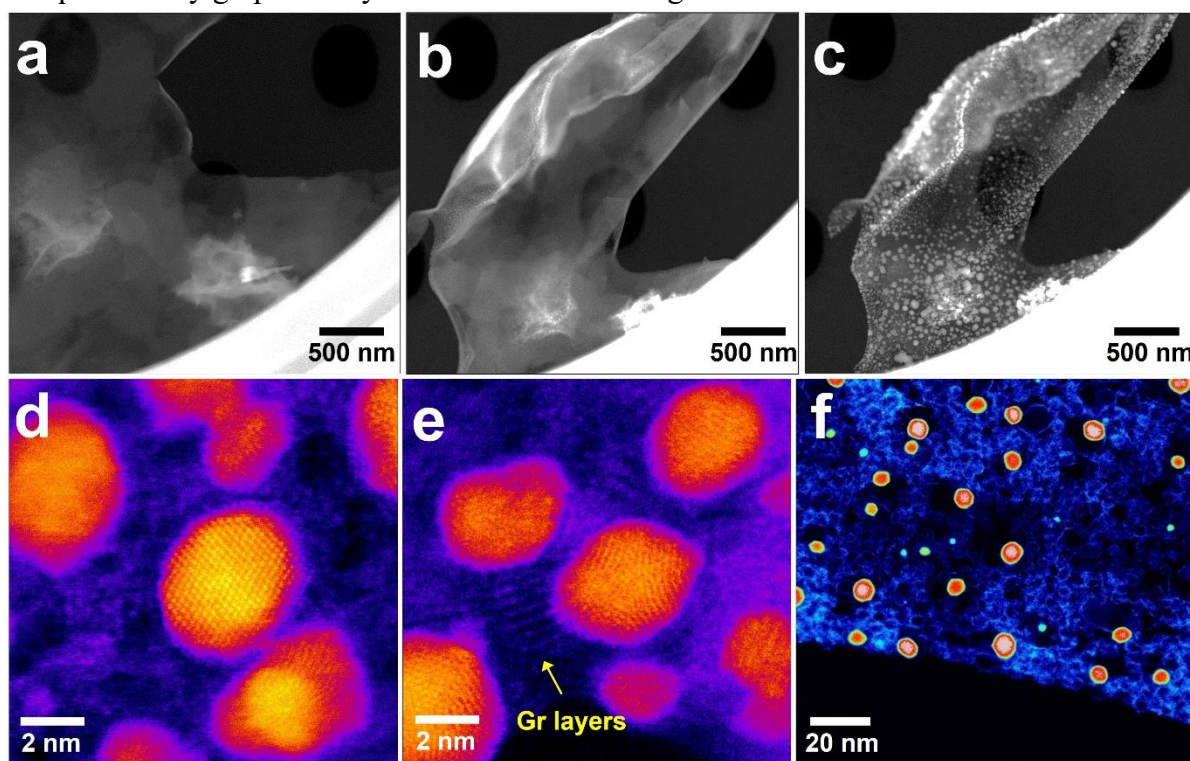


**Figure 2.** (a)-(c) Successive HAADF-STEM images showing the transformation (d) and (e) HAADF-STEM images showing the Co particles with thin carbon film at 500 °C and 800 °C, respectively. (f) Low-scale HAADF-STEM images showing the Co particles with graphene layers.



We observed an encapsulated Co particle using STEM mode, which allows us to collect various images using bright field (BF), annular dark field (ADF: DF2, DF4), and HAADF detectors simultaneously. Even if the material is composed of the same element, the degree of visualization differs depending on the type of detector used in STEM mode. This is because the detection degree of the scattered electron beam varies according to the scattering angle of the electron beam as it scatters through the material. Therefore, we obtained BF, DF2, DF4, and HAADF images in STEM mode to investigate the morphology and structure of a Co particle encapsulated by graphene layers as shown in Figure 3. The distance between the graphene interlayers is measured to be 0.142 nm, which is consistent with the graphene interplanar spacing.

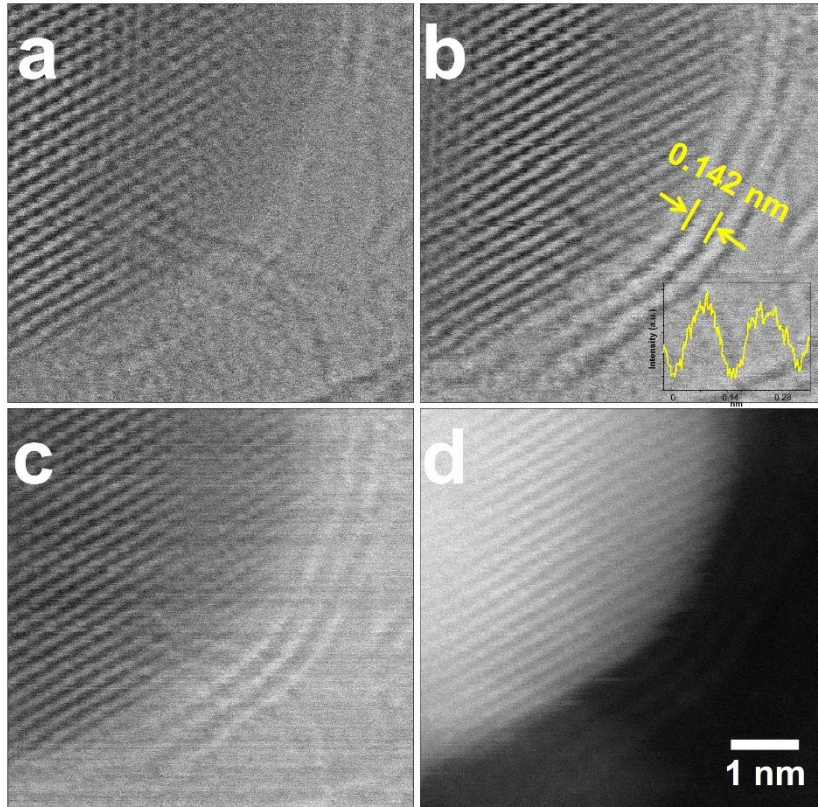


**Figure 3.** Co particle encapsulated by graphene layers, which collected by (a) BF, (b) and (c) ADF and (d) HAADF detectors, respectively.

The graphene layer forms to surround the Co particles, and even if the Co particles partially move, the graphene layer maintains its shape. As shown in Figure 4a, four graphene layers surround the Co particles, and they maintain their morphology while the Co particles move in the direction of the light blue arrow (Figures 4b and c). This result suggests that the graphene layers surrounding the Co particles were not formed temporarily but were formed in a stacked form while maintaining the interlayer spacing with crystallinity. After EDS mapping confirmed the graphene layers remained after the movement of the Co particles, the graphene layers visualized in Figures 4d and e were also included in the entire supported carbon film region, confirming the overall C mapping in the field of view.

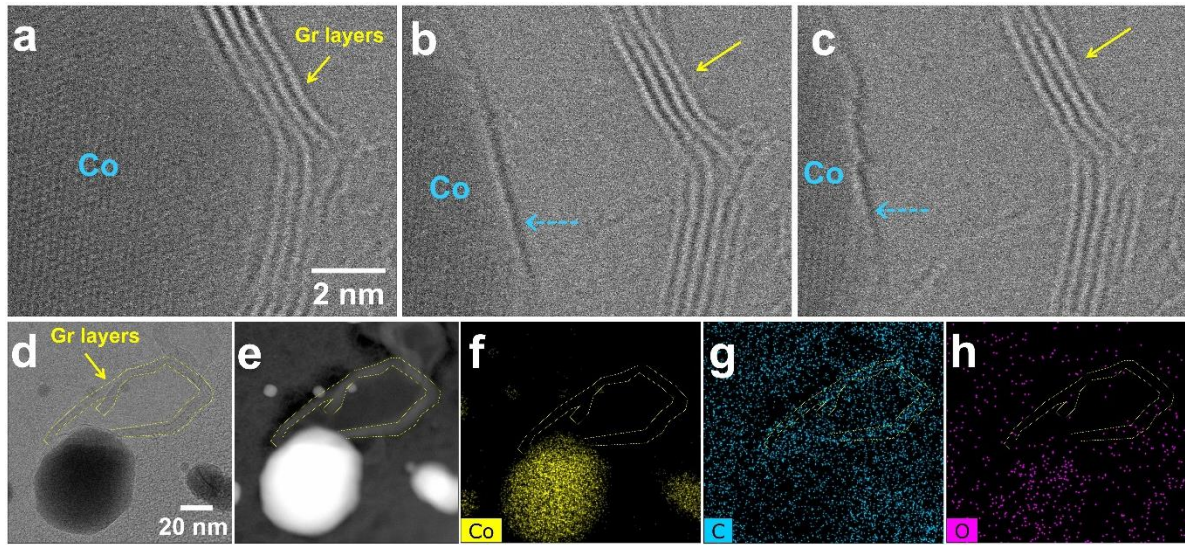


**Figure 4.** (a)-(c) Successive BF-STEM images showing formation of graphene layers surrounding Co particle. (d)-(e) BF and HAADF-STEM images of Co particle and remaining graphene layers. (f)-(h) EDS mapping of Co, C, and O elements at the same region as (d) and (e).

The graphene layer surrounds the Co particles without a gap between the interface of the Co particles and the graphene layer. The number of graphene layers, which are observed prominently at 800 °C or higher, increases when a heating pulse of 1000 °C or higher is applied. Figure 5 shows BF-STEM images of the graphene layers identified encapsulating the Co particle at 1050 °C. The number of graphene layers at the top of the Co particle was 9 (Figure 5a), but when the results of continuous image acquisition were confirmed, the number of layers increased to 12 (Figure 5b). In addition, the number of graphene layers surrounding the lower left part of the Co particle increased from 7 layers to 11 layers (Figure 5c). This is because, as in the case of synthesizing graphene using a metal catalyst, Co particles act as a catalyst, and the remaining amorphous carbon source expands the number of graphene layers at 1000° C or more and is smoothly crystallized into graphene.

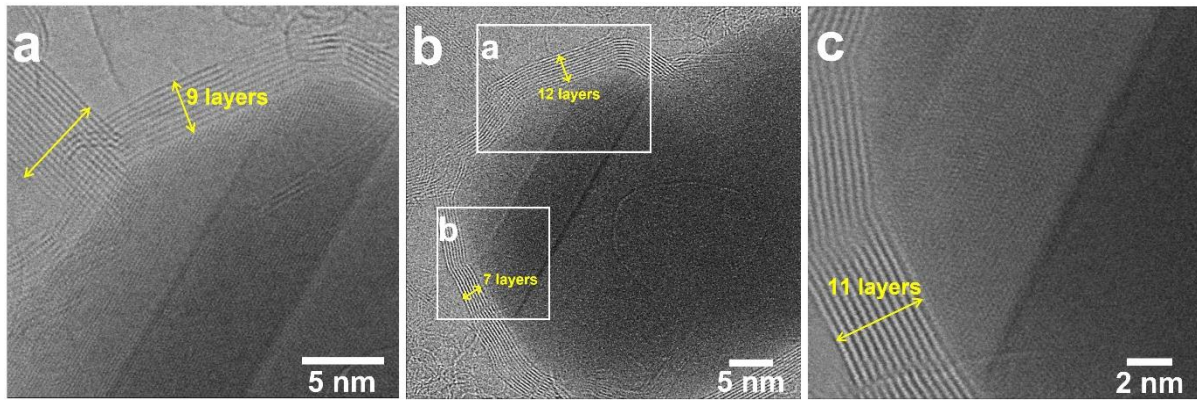


**Figure 5.** Successive BF-STEM images showing the growth of graphene layers at 1050 °C.



## Conclusions

We summarize that the behavior of Co particles encapsulated by graphene layers formed by high temperature and electron beam irradiation. The amorphous carbon remaining in the synthesized  $\text{Co(OH)}_2$  nanosheet exists in the form of a thin film, which crystallizes when a temperature of 800 °C or higher is applied. The crystallized carbon grows into a graphene layer surrounding the Co particles, and the number of graphene layers gradually increases due to the catalytic activation of Co at temperatures above 1000 °C. All these behaviors were observed through STEM imaging, and the graphene layer composed of low elements was observed using BF and ADF images in STEM mode, which has the advantage of using various detectors at the same time. The results of this work show a versatile and scalable technique that can be used to fabricate structured graphene materials.

## Methods

*Synthesis.*  $\text{Co(OH)}_2$  nanosheets were synthesized using the aqueous nutrient solution containing 2 mM cobalt nitrate hexahydrate and 2 mM hexamethylenetetramine (HMTA). Depending on the opening area of a container, a calculated amount of chloroform solution of sodium hexadecyl sulfate (SHS) was added to the water-air interface. After about 30 minutes, the container was capped and placed in a convection oven at 70 °C for typically 180 minutes. The synthesized  $\text{Co(OH)}_2$  sheets were scooped using an TEM grid for imaging.

*Transmission Electron Microscopy.* STEM images were acquired using an aberration-corrected FEI Titan Cubed TEM (FEI Titan3 G2 60-300), which was operated at a 200 kV acceleration voltage with a monochromator.

## List of abbreviations

XPS: X-ray Photoelectron Spectroscopy

SEM: Scanning Electron Microscopy

HAADF-STEM: High Angle Annular Dark Field Scanning Transition Electron Microscopy

ADF: Annular Dark Field

BF: Bright Field

DF: Dark Field

## Declarations

## Availability of data and materials

The datasets used and/or analyzed during the study are available from the corresponding author

on reasonable request.

### **Competing interests**

The authors declare that they have no competing interests.

### **Funding**

This research received no external funding.

### **Author Contribution**

Corresponding E-mail Address: gh.ryu@gnu.ac.kr

### **Acknowledgment**

This work was supported by the National Research Foundation of Korea (NRF) grant funded by the Korea government (MSIT) (No. 2020R1G1A1099542), "Regional Innovation Strategy (RIS)" through the National Research Foundation of Korea (NRF) funded by the Ministry of Education (MOE) (2021RIS-003), and Institute for Basic Science (IBS-R019-D1). KN-KSOM-APPM-1121

### **References**

1. R. V. Jagadeesh, A.-E. Surkus, H. Junge, M.-M. Porl, J. Radnik, J. R. Rabeah, H. Huan, V. Schünemann, A. Brückner, M. Beller. Nanoscale Fe<sub>2</sub>O<sub>3</sub>-based catalysts for selective hydrogenation of nitroarenes to anilines. *Science* **342**, 1073 (2013). <https://doi.org/10.1126/science.1242005>
2. A. Meffre, B. Mehdaoui, V. Connord, J. Carrey, P. F. Fazzini, S. Lachaize, M. Respaud, B. Chaudret. Complex nano-objects displaying both magnetic and catalytic properties: a proof of concept for magnetically induced heterogeneous catalysis. *Nano Lett.* **15**, 3241 (2015). <https://doi.org/10.1021/acs.nanolett.5b00446>
3. R. V. Jagadeesh, H. Junge, M.-M. Pohl, J. Radnik, A. Brückner, M. Beller. Selective oxidation of alcohols to esters using heterogeneous Co<sub>3</sub>O<sub>4</sub>-N@C catalysts under mild conditions. *J. Am. Chem. Soc.* **135**, 10776 (2013). <https://doi.org/10.1021/ja403615c>
4. W. M. Czaplik, J.-M. Neudörfl, A. J. v. Wangelin. On the quantitative recycling of Raney–Nickel catalysts on a lab-scale. *Green Chem.* **9**, 1163 (2007). <https://doi.org/10.1039/B708057C>
5. U. L. Zhang, L. Wang, H.-C. Zhang, Y. Liu, H.-Y. Wang, Z.-H. Kang, S.-T. Lee. Graphitic carbon quantum dots as a fluorescent sensing platform for highly efficient detection of Fe<sup>3+</sup> ions. *RSC Adv.* **3**, 3733 (2013). <https://doi.org/10.1039/C3RA23410J>
6. M. R. Friedfeld, M. Shevlin, J. M. Hoyt, S. W. Krska, M. T. Tudge, P. J. Chirik. Cobalt precursors for high-throughput discovery of base metal asymmetric alkene hydrogenation catalysts. *Science* **342**, 1076 (2013). <https://doi.org/10.1126/science.1243550>

7. R. Rahi, M. Fang, A. Ahmed, R. A. Sánchez-Delgado. Hydrogenation of quinolines, alkenes, and biodiesel by palladium nanoparticles supported on magnesium oxide. *Dalton Trans.* **41**, 14490 (2012). <https://doi.org/10.1039/C2DT31533E>
8. Y. Le, X. Xu, P. Zhang, Y. Gong, H. Li, Y. Wang. Highly selective Pd@mpg-C<sub>3</sub>N<sub>4</sub> catalyst for phenolhydrogenation in aqueous phase. *RSC Adv.* **3**, 10973 (2013). <https://doi.org/10.1039/C3RA41397G>
9. D. Ren, L. He, R.-S. Ding, Y.-M. Liu, Y. Cao, H.-Y. He, K.-N. Fan. An unusual chemoselective hydrogenation of quinoline compounds using supported gold catalysts. *J. Am. Chem. Soc.* **134**, 17592 (2012). <https://doi.org/10.1021/ja3066978>
10. M. Yan, T. Jin, Q. Chen, H. E. Ho, T. Fujita, L.-Y. Chen, M. Bao, M.-W. Chen, N. Asao, Y. Yamamoto. Unsupported nanoporous gold catalyst for highly selective hydrogenation of quinolines. *Org. Lett.* **15**, 1484 (2013). <https://doi.org/10.1021/ol400229z>
11. D. Ge, L. Hu, J. Wang, X. Li, F. Qi, J. Lu, X. Cao, H. Gu. Reversible hydrogenation–oxidative dehydrogenation of quinolines over a highly active Pt nanowire catalyst under mild conditions. *ChemCatChem* **5**, 2183 (2013). <https://doi.org/10.1002/cctc.201300136>
12. A. Corma, P. Serna, P. Concepción, J. J. Calvino. Transforming nonselective into chemoselective metal catalysts for the hydrogenation of substituted nitroaromatics. *J. Am. Chem. Soc.* **130**, 8748 (2008). <https://doi.org/10.1021/ja800959g>
13. G. M. Sammis, H. Danjo, E. N. Jacobsen. Cooperative dual catalysis: application to the highly enantioselective conjugate cyanation of unsaturated imides. *J. Am. Chem. Soc.* **126**, 9928 (2004). <https://doi.org/10.1021/ja046653n>
14. M. Toyofuku, S.-i. Fujiwara, T. Shin-ike, H. Kuniyasu, N. Kambe. Platinum-catalyzed intramolecular vinylchalcogenation of alkynes with  $\beta$ -phenylchalcogeno conjugated amides. *J. Am. Chem. Soc.* **130**, 10504 (2008). <https://doi.org/10.1021/ja804121j>
15. A. S. K. Hashmi, C. an Lothschütz, R. Döpp, M. Rudolph, T. D. Ramamurthi, F. Rominger. Gold and palladium combined for cross-coupling. *Angew. Chem. Int. Ed.* **48**, 8243 (2009). <https://doi.org/10.1021/ja400311h>
16. R. Chinchilla, C. Nájera. The sonogashira reaction: a booming methodology in synthetic organic chemistry. *Chem. Rev.* **107**, 874 (2007). <https://doi.org/10.1021/cr050992x>
17. Y. Yao, Q. Fu, Y. Y. Zhang, X. Weng, H. Li, M. Chen, L. Jin, A. Dong, R. Mu, P. Jiang, L. Liu, H. Bluhm, Z. Liu, S. B. Zhang, X. Bao. Graphene cover-promoted metal-catalyzed reactions. *Proc. Natl. Acad. Sci. USA* **111**, 17023 (2014). <https://doi.org/10.1073/pnas.1416368111>
18. V. R. Galakhov, A. S. Shkvarin, A. S. Semenova, M. A. Uimin, A. A. Mysik, N. N. Shchegoleva, A. Ye. Yermakov, E. Z. Kurmaev. Characterization of carbon-encapsulated nickel and iron nanoparticles by means of X-ray absorption and photoelectron spectroscopy. *J. Phys. Chem. C* **114**, 22413 (2010). <https://doi.org/10.1021/jp106612b>

19. R. Liu, S. M. Mahurin, C. Li, R. R. Unocic, J. C. Idrobo, H. Gao, S. J. Pennycook, S. Dai. Dopamine as a carbon source: the controlled synthesis of hollow carbon spheres and yolk-structured carbon nanocomposites. *Angew. Chem. Int. Ed. Engl.* **50**, 6799 (2011). <https://doi.org/10.1002/anie.201102070>
20. L. Chen, H. Chen, R. Luque, Y. Li. Metal–organic framework encapsulated Pd nanoparticles: towards advanced heterogeneous catalysts. *Chem. Sci.* **5**, 3708 (2014). <https://doi.org/10.1039/C4SC01847H>
21. H. Tian, X. Li, L. Zeng, J. Gong. Recent advances on the design of group VIII base-metal catalysts with encapsulated structures. *ACS Catal.* **5**, 4959 (2015). <https://doi.org/10.1021/acscatal.5b01221>
22. X. Wu, H. niu, S. Fu, J. Song, C. Mao, S. Zhang, D. Zhang, C. Chen. Core–shell CeO<sub>2</sub>@C nanospheres as enhanced anode materials for lithium ion batteries. *J. Mater. Chem. A* **2**, 6790 (2014). <https://doi.org/10.1039/C3TA15420C>
23. Z. Wei, Y. Chen, J. Wang, D. Su, M. Tang, S. Mao, Y. Wang. Cobalt encapsulated in N-doped graphene layers: an efficient and stable catalyst for hydrogenation of quinoline compounds. *ACS Catal.* **6**, 5816 (2016). <https://doi.org/10.1021/acscatal.6b01240>
24. Y. L. Liu, X. Y. Xu, P. C. Sun, T. H. Chen. N-doped porous carbon nanosheets with embedded iron carbide nanoparticles for oxygen reduction reaction in acidic media, *Int. J. Hydrogen Energy* **40**, 4531 (2015). <https://doi.org/10.1039/C6RA27826D>
25. L. Peng, S. Yang, S. B. EmadOveisi, D. T. Sun, M. Asgari, O. Trukhina, W. L. Queen. MOF-derived cobalt phosphide carbon nanocubes for selective hydrogenation of nitroarenes to anilines, *ChemPubSoc* **24**, 4234 (2018). <https://doi.org/10.1039/C5RA17427A>
26. Z. Wei, J. Wang, S. Mao, D. Su, H. Jin, Y. Wang, F. Xu, H. Li, Y. Wang. In situ-generated Co<sub>0</sub>-Co<sub>3</sub>O<sub>4</sub>/N-doped carbon nanotubes hybrids as efficient and chemoselective catalysts for hydrogenation of nitroarenes, *ACS Catal.* **5**, 4783 (2015). <https://doi.org/10.1021/acscatal.5b00737>
27. R. Rosei, S. Modesti, F. Sette, C. Quaresima, A. Savoia, P. Perfetti. Electronic structure of carbidic and graphitic carbon on Ni(111). *Phys. Rev. B* **29**, 3416 (1984). <https://doi.org/10.1103/PhysRevB.29.3416>
28. A. Nagashima, N. Tejima, C. Oshima. Electronic states of the pristine and alkali-metal-intercalated monolayer graphite/Ni(111) systems. *Phys. Rev. B* **50**, 17487 (1994). <https://doi.org/10.1103/PhysRevB.50.17487>
29. Y. Gamo, A. Nagashima, M. Wakabayashi, M. Terai, C. Oshima. Atomic structure of monolayer graphite formed on Ni(111). *Surf. Sci.* **374**, 61 (1997). [https://doi.org/10.1016/S0039-6028\(96\)00785-6](https://doi.org/10.1016/S0039-6028(96)00785-6)



30. F. Abild-Pedersen, J. K. Nørskov, J. R. Rostrup-Nielsen, J. Sehested, S. Helveg. Mechanisms for catalytic carbon nanofiber growth studied by ab initio density functional theory calculations. *Phys. Rev. B* **73**, 1 (2006). <https://doi.org/10.1103/PhysRevB.73.115419>
31. S.-G. Wang, X. Y. Liao, D. B. Cao, Y. W. Li, J. Wang, H. Jiao. Formation of carbon species on Ni(111): structure and stability. *J. Phys. Chem. C* **111**, 10894 (2007). <https://doi.org/10.1021/jp070608v>
32. A. Gruneis, D. V. Vyalikh. Tunable hybridization between electronic states of graphene and a metal surface. *Phys. Rev. B* **77**, 93401(2008). <https://doi.org/10.1021/acs.jpcc.5b05428>